

# LMOD: A Large Multimodal Ophthalmology Dataset and Benchmark for Large Vision-Language Models

Zhenyue Qin<sup>1\*</sup> Yu Yin<sup>2\*</sup> Dylan Campbell<sup>3</sup> Xuansheng Wu<sup>4</sup>

Ke Zou<sup>5</sup> Yih-Chung Tham<sup>5</sup> Ninghao Liu<sup>4</sup> Xiuzhen Zhang<sup>6</sup> Qingyu Chen<sup>1†</sup>

<sup>1</sup>Yale University <sup>2</sup>Imperial College London <sup>3</sup>Australian National University

<sup>4</sup>University of Georgia <sup>5</sup>National University of Singapore <sup>6</sup>RMIT University

## Abstract

Ophthalmology relies heavily on image analysis for diagnosis and treatment planning. While large vision-language models (LVLMs) have shown promise in understanding complex visual information, their performance on ophthalmology images remains underexplored. We introduce LMOD, a dataset and benchmark for evaluating LVLMs on ophthalmology images, covering anatomical understanding and diagnostic analysis. LMOD includes 21,933 images spanning optical coherence tomography, scanning laser ophthalmoscopy, eye photos, surgical scenes, and color fundus photographs. We benchmark 13 state-of-the-art LVLMs and find that they are far from perfect for comprehending ophthalmology images. In anatomical recognition, models struggle with spatial reasoning, particularly in complex images with multiple bounding boxes, and exhibit inconsistent performance across different datasets. For diagnostic analysis, models perform close to random guessing in glaucoma detection and achieve limited accuracy in macular hole staging. Our error analysis uncovers six primary failure modes in diagnostic analysis: misclassification, failure to abstain, inconsistent reasoning, hallucination, assertion without explanation, and lack of domain-specific knowledge.

## 1 Introduction

The ever-increasing prevalence of primary eye diseases poses a significant global burden (Tham et al., 2014; Neely et al., 2017; Cavan et al., 2017). More than 2.2 billion individuals suffer from vision impairment worldwide, with disproportionately higher rates in low- and middle-income regions (Organization, 2023). Limited access to comprehensive eye examinations, along with a shortage of clinicians, results in a substantial proportion of major eye diseases being undiagnosed or diagnosed

\* Equal contribution

† Correspondence email: qingyu.chen@yale.edu



**Figure 1: Failure to abstain from making predictions on out-of-domain images.** The figure illustrates the responses generated by LLaVA-Med and InternVL-2B when presented with a non-ophthalmology image of a cat and queried about the presence of glaucoma. Despite the image being outside the domain of fundus photography, LLaVA-Med incorrectly classifies the cat image as showing signs of glaucoma. Similarly, InternVL-2B misinterprets the cat image as a fundus image but concludes that there are no signs of glaucoma based on the visible features.

too late for effective treatment (Neely et al., 2017; Varma et al., 2011). To address this challenge, artificial intelligence (AI) applications have been developed to streamline clinical workflows by assisting in patient triage, disease diagnosis, prognosis prediction, and reducing documentation burdens (Ting et al., 2019; Peng et al., 2019; Keenan et al., 2022; De Fauw et al., 2018; Zhou et al., 2023; Kaushal et al., 2023; Elkholy and Marzouk, 2024).

Recent advancements in AI, particularly Large Language Models (LLMs), have garnered significant attention. Notably, they show potential in medical applications (Tian et al., 2024; Chen et al., 2023; Qin et al., 2022). In addition, their multimodal extensions enable LLMs to capture diverse representations and process information from mul-

multiple modalities, which are crucial in clinical practice. For example, GPT-4o (Achiam et al., 2023) and LLaVA (Liu et al., 2024) combine LLMs with vision encoders to allow models generate responses based on input images. Such capabilities are particularly beneficial in medical imaging, where interpretations and follow-up plans are documented in free-text clinical notes (Tian et al., 2024; Xiao et al., 2024).

Specifically, in ophthalmology, LVLMs enable automated disease diagnosis and classification, such as assessing the severity level of glaucoma, region classification and segmentation, such as segmenting retinal nerve fiber layers in optical coherence tomography (OCT), and documentation, such as generating free-text imaging interpretations (Betzler et al., 2023). Importantly, what distinguishes LVLMs is their ability to handle these tasks within a single model using zero- or few-shot learning. In contrast, previous applications required sophisticated fine-tuning on substantial manually curated instances, making it challenging to adapt fine-tuned models to different data types (Xiao et al., 2024; Betzler et al., 2023). This may improve the efficiency and accuracy of workflows in ophthalmology clinics (De Fauw et al., 2018).

Nevertheless, to date, limited benchmarks are available to assess LVLMs in ophthalmology-specific applications, and consequently, the potential and limitations of LVLMs are not clear. Existing studies in ophthalmology focus on evaluating the performance of LLMs on text-based tasks, including multiple-choice questions (Wu et al., 2024), general ophthalmology knowledge testing (Antaki et al., 2023), and free-text question answering on specific ophthalmology topics (Lim et al., 2023). While these studies are useful for demonstrating potential, ophthalmic images are arguably the most important data modality. Ophthalmologists require different imaging modalities for diagnosis and prognosis that are not derived from the text itself (Khan et al., 2021). Therefore, the capability of image analysis is crucial in the domain of ophthalmology. In addition, existing ophthalmic imaging datasets were designed for the development and evaluation of fine-tuning AI models; they may only contain a single imaging modality (e.g., OCT only), a specific task (e.g., region segmentation), and specific output types (e.g., a disease severity class rather than free text).

In response, this study proposes a systematic and reproducible data and evaluation pipeline that re-

purposes existing datasets to curate a dataset we refer to as LMOD (Large Multimodal Ophthalmology Dataset) for the development and evaluation of LVLMs in ophthalmology. LMOD consists of five ophthalmic imaging modalities: OCT, CFP, scanning laser ophthalmoscopy (SLO), lens photographs, and surgical scenes, along with biomarkers and free text, collectively comprising over 20K instances. It also provides multi-granular annotations, including region annotation and disease information. The pipeline can also be directly applied to new datasets.

We further systematically assess 13 state-of-the-art LVLMs on (1) anatomical recognition, which quantifies the effectiveness of LVLMs at the region level (Demer, 2006) and (2) disease diagnosis and classification, which quantifies the effectiveness of LVLMs for ophthalmic diseases, and (3) demographic information extraction to assess whether LVLMs can infer demographic variables such as age and gender from ophthalmic images, as previous studies have found in AI models for retinal scans (Poplin et al., 2018).

Our contributions are as follows:

- We introduce LMOD, a large-scale ophthalmology dataset that includes over 21K images across diverse imaging modalities. LMOD is richly annotated with disease labels and bounding boxes, supporting comprehensive evaluations from macro-level image diagnosis to micro-level anatomical recognition.
- We benchmark 13 state-of-the-art (SoTA) LVLMs, including models with diverse visual backbones and LLMs. The evaluation is conducted using a wide range of metrics, assessing strengths and weaknesses of LVLMs from various perspectives.
- We conduct comprehensive evaluations and through error analysis, combining both high-level overview and nuanced analyses, through various result presentation forms, such as weighted averages, bar and radar charts, as well as visual illustrations.

## 2 Related Work

### 2.1 Advances in Large Vision-Language Models

The release of ChatGPT (Achiam et al., 2023) has sparked considerable interest in the potential of

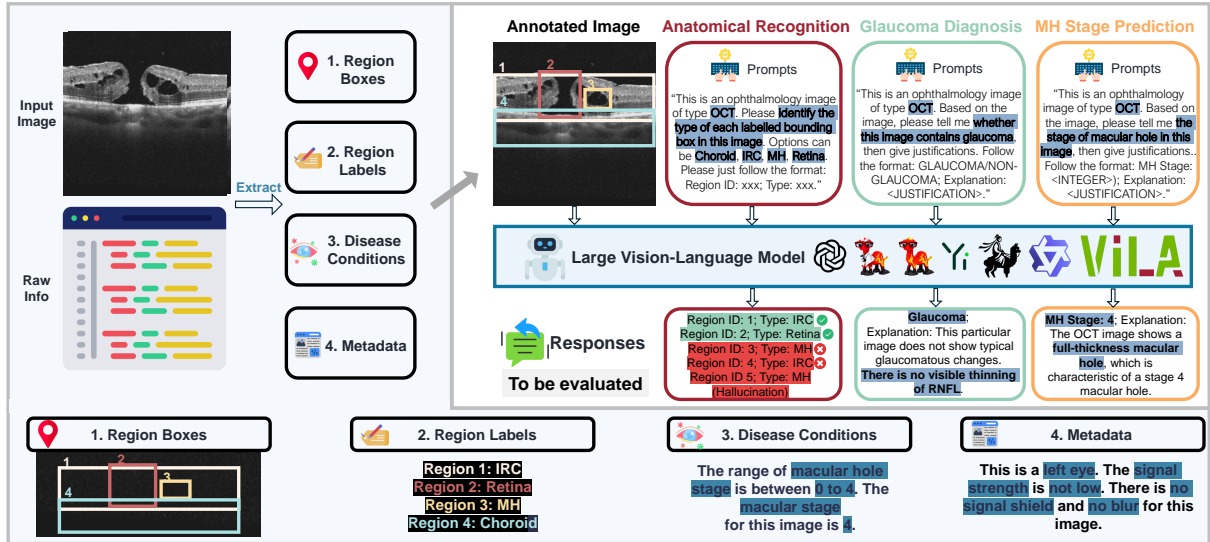


Figure 2: Overview of our data processing and evaluation pipeline for assessing the performance of large vision-language models (LVLMs) on box-annotated ophthalmology images. The input image is preprocessed to extract raw information such as bounding boxes, labels, patient metadata, and disease conditions. This aggregated information is then used to generate a structured prompt that includes a description of the image type and instructions for the LVLM to identify the type of each labeled region. The LVLM processes the input image and prompt to generate a response categorizing each region. Finally, the model’s output is compared against the ground truth labels using our proposed evaluation metrics to quantify the LVLM’s performance in understanding and analyzing the detailed visual information in ophthalmology images.

Benchmarks	Modalities		Image Types					Evaluation Perspectives		
	Images	Texts	Surgical Scenes	SLO	OCT	Eye Photos	Fundus Images	Anatomical Understanding	Diagnosis Analysis	Biomarker Prediction
General-Domain Benchmarks										
MMMU (Yue et al., 2024)	✓	✓	✗	✗	✗	✓	✓	✗	✗	✗
MME-RealWorld (Zhang et al., 2024b)	✓	✓	✗	✗	✗	✗	✗	✗	✗	✗
UNK-VQA (Guo et al., 2024)	✓	✓	✗	✗	✗	✗	✗	✗	✗	✗
MMC-Bench (Zhang et al., 2024a)	✓	✓	✗	✗	✗	✗	✗	✗	✗	✗
MathVista (Lu et al., 2023)	✓	✓	✗	✗	✗	✗	✗	✗	✗	✗
SEED-Bench (Li et al., 2024a)	✓	✓	✗	✗	✗	✗	✗	✗	✗	✗
Ophthalmology-Specific Benchmarks										
Bench-Nephrology (Wu et al., 2024)	✗	✓	✗	✗	✗	✗	✗	✗	✗	✗
Eval-GPT-Ophth (Antaki et al., 2023)	✗	✓	✗	✗	✗	✗	✗	✗	✗	✗
Bench-Myopia (Lim et al., 2023)	✗	✓	✗	✗	✗	✗	✗	✗	✗	✗
OphNet (Hu et al., 2024)	✓	✓	✓	✗	✗	✗	✗	✗	✗	✗
<b>LMOD (ours)</b>	✓	✓	✓	✓	✓	✓	✓	✓	✓	✓

Table 1: Comparison of existing general-domain and ophthalmology-specific benchmarks for evaluating large vision-language models, highlighting their supported modalities, coverage of image types, and evaluation perspectives.

large language models (LLMs) across various domains (Liu et al., 2023; Tian et al., 2024; De Angelis et al., 2023). Building on the success of ChatGPT and other LLMs (Radford et al., 2018, 2019; Brown et al., 2020), researchers have developed large vision-language models (LVLMs) that integrate the strengths of vision encoders with LLMs. These vision encoders are typically pretrained on vast image datasets in an unsupervised manner, such as randomly masking parts of an image and

training the encoder to reconstruct the missing sections. These models employ vision encoders to extract visual features from images and incorporate them into LLMs, enabling a combined understanding of both vision and language. The advent of LVLMs has opened up new possibilities for multimodal reasoning and comprehension, with applications spanning various fields, including the medical domain (Clusmann et al., 2023; Kung et al., 2023; Currie et al., 2023; Qin et al., 2022).

Several notable LVLMs have been introduced in recent years, each with its unique architecture and training approach. GPT-4 (Achiam et al., 2023), developed by OpenAI, has demonstrated remarkable performance across a wide range of tasks, including visual question answering (Antol et al., 2015; Goyal et al., 2017) and image captioning (Lin et al., 2014). LLaVA (Liu et al., 2024) is another LVLM that leverages a pre-trained vision encoder and a large language model to achieve state-of-the-art performance on various vision-language tasks. Similarly, InternVL (Chen et al., 2024) employs a vision transformer and a language model to learn joint representations of images and text. QWEN (Bai et al., 2023) utilizes a query-based approach to align visual and textual representations, while VILA (Lin et al., 2023) introduces a novel architecture that integrates visual and linguistic information at multiple levels to enhance the model’s understanding of both modalities. In the medical domain, representative LVLMs include LLaVA-Med and its variants (Li et al., 2024b; Jiang et al., 2024; Xie et al., 2024). These models use LLaVA as the backbone, are further fine-tuned on large-scale medical images and text, and demonstrate potential for disease diagnosis and medical question answering (Li et al., 2024b).

## 2.2 Lack of Benchmarks for the Development and Evaluation of LVLMs in Ophthalmology

In ophthalmology, studies have demonstrated the utility of domain-specific foundation models. For example, several vision encoders pretrained on ophthalmic images have shown consistent improvements in diagnosing and predicting the prognosis of eye diseases (Zhou et al., 2023; Kaushal et al., 2023; Elkholy and Marzouk, 2024). However, vision encoders alone lack the reasoning and conversational capabilities inherent to large language models (LLMs). These encoders require task-specific fine-tuning with static inputs and outputs. Furthermore, as noted earlier, existing research on LLMs in ophthalmology is primarily focused on text-based applications, such as multiple-choice questions and knowledge testing (Wu et al., 2024; Antaki et al., 2023; Lim et al., 2023), neglecting ophthalmic images as a key data modality.

To the best of our knowledge, few benchmarks exist for the development and evaluation of LVLMs in ophthalmology. This lack of benchmarks poses a significant barrier to systemati-

cally evaluating the feasibility of applying existing LVLMs in this domain and hinders the development of ophthalmology-specific LVLMs. This is particularly inefficient given that vision encoders for ophthalmology are already available. In contrast, several benchmarks have been established in both general and medical domains. Table 1 categorizes these benchmarks by data modality and downstream evaluation tasks. For example, the MMMU benchmark (Yue et al., 2024) provides a comprehensive evaluation of LVLMs on college examination questions across multiple disciplines, assessing their understanding and reasoning capabilities. Similarly, Bench-Nephrology (Wu et al., 2024) serves as a nephrology-specific benchmark for LVLMs. However, existing benchmarks in ophthalmology are primarily designed for the development and evaluation of AI models under the finetuning paradigm, rather than for LVLMs. These benchmarks often focus on a single imaging modality (e.g., OCT only), a specific task (e.g., region segmentation), and restricted output types (e.g., disease severity classification rather than free-text outputs). As shown in Table 1, few benchmarks encompass diverse ophthalmic imaging modalities or support a broad range of downstream evaluations. These evaluations may include anatomical understanding, which involves the accurate identification and localization of ocular structures (Wang et al., 2021; De Fauw et al., 2018), diagnostic analysis, which requires the interpretation of visual features and patterns to assess the presence and severity of ocular diseases, and systemic biomarker prediction, which focuses on the extraction of systemic risk factors and demographic variables.

## 3 LMOD Curation

In this section, we present our methodology for curating LMOD: Large Multimodal Ophthalmology Dataset. We first describe our data curation pipeline, which involves selecting suitable datasets, generating consistent annotations across various image types, and designing standardized prompts for model evaluation. Next, we introduce the evaluation tasks and metrics used to assess the performance of LVLMs on LMOD, focusing on anatomical recognition and diagnostic analysis.

### 3.1 Data Curation Pipeline

**Step 1: Dataset Selection.** We screened and selected the datasets for repurposing based on the

---

**Algorithm 1** Anatomical Recognition Pipeline
 

---

**Require:** Original dataset  $D = \{(I_1, R_1), (I_2, R_2), \dots, (I_n, R_n)\}$ , where  $I_i$  is an image and  $R_i$  is the corresponding raw data

**Require:** Minimum bounding box area threshold  $\tau \in \mathbb{R}^+$

**Ensure:** Curated dataset  $D' = \{(I_1, B'_1, P_1), (I_2, B'_2, P_2), \dots, (I_n, B'_n, P_n)\}$ , where  $B'_i$  is the set of curated bounding boxes and  $P_i$  is the set of corresponding prompts for image  $I_i$

- 1: **for** each image-raw data pair  $(I_i, R_i) \in D$  **do**
- 2:    $B_i \leftarrow \text{ExtractBoundingBoxes}(R_i)$ , where  $B_i = \{b_{i,1}, b_{i,2}, \dots, b_{i,|B_i|}\}$  and  $b_{i,j}$  is the  $j$ -th bounding box of image  $I_i$
- 3: **end for**
- 4:  $B \leftarrow \bigcup_{i=1}^n B_i$
- 5:  $B' \leftarrow \{b \in B \mid \text{area}(b) \geq \tau\}$
- 6: **for** each image-raw data pair  $(I_i, R_i) \in D$  **do**
- 7:    $B'_i \leftarrow \{b \in B' \mid b \text{ belongs to image } I_i\}$
- 8:    $P_i \leftarrow \emptyset$
- 9:   **for** each bounding box  $b_{i,j} \in B'_i$  **do**
- 10:      $id_{i,j} \leftarrow \text{GenerateUniqueID}()$
- 11:      $color_{i,j} \leftarrow \text{AssignDistinctColor}()$
- 12:      $prompt_{i,j} \leftarrow \text{GeneratePrompt}(b_{i,j})$
- 13:      $P_i \leftarrow P_i \cup \{(id_{i,j}, color_{i,j}, prompt_{i,j})\}$
- 14:   **end for**
- 15: **end for**
- 16: **return**  $D'$

---

Data Types	Num Images	Num Avg Boxes
Surgical Scenes (SS)	2,256	3.3
Optical Coherence Tomography (OCT)	3,859	2.4
Scanning Laser Ophthalmoscopy (SLO)	10,000	1.0
Eye Photos (EP)	2,432	1.9
Color Fundus Images (CFI)	3,386	1.6

Table 2: Overview of LMOD, including the number of images (Num Images) and average number of bounding boxes per image (Num Avg Boxes) for each data type.

following criteria:

- **Accessibility:** The datasets are publicly accessible and non-copyrighted, ensuring that LMOD can be widely used by the research community for model evaluation and development.
- **Coverage:** The datasets collectively needed to cover key ophthalmic imaging modalities and primary eye diseases.
- **Diversity:** Population diversity was considered, enabling the benchmarks to quantify model effectiveness across subgroups, especially within disparity populations.

As a result, nine datasets were selected for curation. These datasets can be categorized into five ophthalmic imaging types:

- **SS:** SS stands for surgical scenes. This category includes the Cataract-1K dataset (Ghamsarian et al., 2024), which contains 2,256 images extracted from cataract surgery videos. These images capture various stages and aspects of the

surgical procedure, with an average of 3.3 bounding boxes per image.

- **OCT:** OCT represents Optical Coherence Tomography. The OIMHS dataset (Ye et al., 2023) represents this category, comprising 3,859 OCT images. OCT is a non-invasive imaging technique that provides high-resolution cross-sectional images of the retina. On average, each image contains 2.4 bounding boxes.

- **SLO:** SLO indicates Scanning Laser Ophthalmoscopy. The Harvard FairSeg dataset (Luo et al., 2024) is included in this category, featuring 10,000 SLO fundus images. Each image contains an average of one bounding box.

- **EP:** EP means Eye Photographs. This category includes two datasets: CAU001 (PupiUp, 2023) and Cataract Detection 2 (Ramapuram, 2023). CAU001 contains 1,417 RGB photographs of human eye regions, with bounding box annotations indicating the locations of the left and right eyes, pupils, and irises. Cataract Detection 2 consists of 1,015 photographs of eyes with and without cataracts, each containing a single bounding box annotation. The average number of bounding boxes per image is 1.9.

- **CFP:** CFP implies Color Fundus Photographs. This category includes four datasets: REFUGE (Orlando et al., 2020), IDRiD (Prasanna et al., 2018), ORIGA (Zhang et al., 2010), and G1020 (Bajwa et al., 2020). REFUGE contains 1,200 retinal fundus images, including both glaucoma and normal eyes, with detailed annotations of optic disc and cup segmentations. IDRiD includes 516 images with pixel-level annotations of typical diabetic retinopathy lesions and normal retinal structures. ORIGA consists of 650 retinal images annotated by trained professionals, containing a comprehensive set of image features critical for glaucoma diagnosis. G1020 contains 1,020 high-resolution color fundus photographs, accompanied by detailed ground-truth annotations, including glaucoma diagnosis, optic disc and cup segmentations, and other clinically relevant measurements. On average, each image in this category contains 1.6 bounding boxes.

**Step 2: Multigranular Annotation.** We further curated the datasets to support the development and evaluation of LVLMs in ophthalmology applications. These applications are categorized into two main parts: (1) anatomical understanding, which

involves the accurate identification and localization of ocular structures (Wang et al., 2021; De Fauw et al., 2018), and (2) diagnostic analysis, which requires the interpretation of visual features and patterns to assess the presence and severity of ocular diseases. The curation for each application is detailed below.

**Anatomical Recognition:** Anatomical recognition refers to the ability of models to accurately identify various anatomical structures in ophthalmology images. The overall pipeline is algorithmically outlined in [Algorithm 1](#). In brief, the steps are as follows: First, we generate bounding boxes and their associated labels. The coordinates of the bounding boxes are present in the open-source datasets. To ensure consistency and standardization across the dataset, we map the region types provided in the open-source datasets to a predefined set of ophthalmology-specific region types, such as optic disk, macula, lesion, and tumor. This mapping process allows us to handle variations in terminology and granularity used in the original datasets.

To balance between the comprehensiveness of annotations and the clarity of the images, we establish a threshold and remove bounding boxes whose areas fall below this threshold. This step is crucial for two reasons. First, an excessive number of bounding boxes overlaid on the images can lead to significant occlusion, hindering the visibility and interpretability of the underlying image content. Second, the presence of numerous small bounding boxes can result in a disproportionate ratio between the number of text IDs and the number of bounding boxes, making it challenging to establish a clear association between the two.

In the final step, using the extracted bounding box coordinates, we generate visual markers in the form of bounding boxes on the images to highlight the annotated regions. These visual markers are assigned unique labels (e.g., letters or numbers) to clearly identify each region. To increase the differentiation between regions, we assign different colors to the bounding boxes.

We formatted the prompts for the models using the following template:

This is an image [IMAGE DESCRIPTION] of type [IMAGE TYPE]. Please identify the type of each labeled bounding box in this image. Options can be: [REGION TYPE 1], [REGION TYPE 2], ... Please just follow the format: Region ID: xxx; Type: xxx.

**Diagnostic Analysis:** We evaluate models' ability to determine the presence and severity of eye diseases, using glaucoma and macular holes as case studies.

Glaucoma is a group of eye diseases that can cause vision loss and blindness by damaging the optic nerve. We formulate glaucoma detection as a binary classification problem, assessing models' performance in predicting the presence or absence of glaucoma based on the visual characteristics of the optic nerve head. The prompt for this task is as follows:

This is <IMAGE TYPE>. Based on the image, please tell me whether this image contains glaucoma, then give justifications. Follow the format: GLAUCOMA / NON-GLAUCOMA; Explanation: <JUSTIFICATION>.

Macular holes, a sight-threatening condition, are classified into five distinct stages, ranging from 0 to 4, based on their size and morphology. Stage 0 represents a normal macula, while stages 1 to 4 indicate increasing severity, with stage 4 being the most advanced and potentially irreversible. We formulate macular hole staging as a classification problem, assessing models' performance in predicting the correct stage based on the visual characteristics of the macular hole. The prompt for this task is as follows:

This is <IMAGE TYPE>. Based on the image, please tell me the stage of the macular hole, then give justifications. Follow the format: Stage: <AN INTEGER>; Explanation: <JUSTIFICATIONS>.

Accuracy serves as the primary evaluation metric for both tasks, quantifying the proportion of correctly classified glaucoma cases and macular hole stages. This approach allows for a direct and meaningful assessment of models' diagnostic capabilities in the context of these two common eye diseases.

To ensure reliability and validity, we extract glaucoma and macular hole labels from the original datasets when available. In cases of imbalanced label distribution, we employ a balanced sampling strategy to mitigate potential biases and ensure fair evaluation. Specifically, we determine the minimum number of samples across all classes and randomly select an equal number of samples from each class to create a balanced dataset. This approach guarantees that models are evaluated on a representative and unbiased sample, preventing

them from exploiting class imbalance and enabling a more accurate assessment of their diagnostic performance.

Models	Anatomical Recognition				Diagnosis Analysis	
	Precision $\uparrow$	Recall $\uparrow$	F1 $\uparrow$	PPV $\uparrow$	Glaucoma Acc (%) $\uparrow$	MH Stage Acc (%) $\uparrow$
Random	-	-	-	-	50.00	20.00
GPT-4o	0.5609	<b>0.5896</b>	<b>0.5748</b>	0.9513	<b>54.09</b>	<b>58.97</b>
LLaVA-Med	0.0789	0.1163	0.0940	0.7435	50.00	25.00
LLaVA-7b	0.0567	0.0410	0.0475	0.2674	50.00	7.30
LLaVA-M-7B	0.1346	0.1450	0.1396	0.7569	50.00	0.00
LLaVA-V-7B	0.3095	0.2540	0.2790	0.7516	50.00	0.00
LLaVA-13B	0.0599	0.0803	0.0686	0.5993	50.00	0.00
Yi-6B	0.1952	0.1499	0.1695	0.8893	50.00	5.26
InternVL-2B	0.6025	0.3999	0.4807	<b>0.9809</b>	50.00	30.26
InternVL-4B	<b>0.7241</b>	0.4481	0.5536	0.9629	50.00	25.00
Qwen	0.0275	0.0372	0.0316	0.8418	50.00	18.42
VILA-3B	0.1429	0.1119	0.0633	0.5300	50.00	24.24
VILA-3B-S2	0.3340	0.2636	0.1255	0.7695	50.00	21.42
VILA-8B	N/A	N/A	N/A	N/A	50.00	22.53
Average	0.2688	0.2197	0.2189	0.7537	50.31	13.44

Table 3: Performance comparison of state-of-the-art large vision-language models on the LMOD benchmark, evaluating their capabilities in anatomical recognition and diagnosis analysis. The best-performing model in each metric is highlighted in bold.

## 4 Benchmarking Results

### 4.1 Benchmarked LVLMs

We benchmarked 13 state-of-the-art large vision-language models on the LMOD benchmark. These models include the following:

- **GPT-4o:** A proprietary model developed by OpenAI (Achiam et al., 2023).
- **LLaVA Variations:** LLaVA (Liu et al., 2024) leverages a pre-trained vision encoder and a large language model to achieve state-of-the-art performance on various vision-language tasks. We evaluate several variations based on different language models and sizes, including LLaVA-7B, LLaVA-M-7B (M for Mistral), LLaVA-V-7B (V for Vicuna), LLaVA-13B, and LLaVA-Med (Li et al., 2024b), which is fine-tuned on a large-scale medical image-text dataset.
- **Yi-6B:** A vision-language model supporting both Chinese and English (Young et al., 2024).
- **InternVL Variations:** InternVL (Chen et al., 2024) aligns a scaled-up vision foundation model with a large language model using web-scale image-text data. We evaluate two variants: InternVL-2B and InternVL-4B.
- **QWen:** A vision-language model that utilizes a query-based approach to align visual and textual representations (Bai et al., 2023).

- **VILA Variations:** VILA focuses on the visual language pre-training process by examining design options for VLM pre-training through augmenting large language models. We evaluate three variants: VILA-1.5-3B, VILA-1.5-3B-S2, and VILA-1.5-8B, with parameter counts ranging from 3 billion to 8 billion (Lin et al., 2023).

### 4.2 Evaluation Metrics

To comprehensively assess the performance of LVLMs on the LMOD benchmark, we employ a set of evaluation metrics that capture different aspects of their capabilities. These metrics are chosen to provide a holistic view of the models’ strengths and weaknesses in analyzing ophthalmology images.

For anatomical recognition, we use the following metrics:

- **Precision:** Measures the proportion of correctly predicted region types among all predicted regions.
- **Recall:** Quantifies the proportion of correctly predicted region types among all ground truth regions.
- **F1 Score:** The harmonic mean of precision and recall, providing a balanced measure of a model’s performance.
- **Positive Predictive Value (PPV):** Represents the proportion of true positive predictions among all positive predictions.

These metrics collectively assess the models’ ability to accurately identify and localize anatomical structures in ophthalmology images.

In the context of diagnostic analysis, we focus on evaluating the models’ performance in glaucoma detection and macular hole staging. For both tasks, we employ the following metric:

- **Accuracy:** Quantifies the proportion of correctly classified glaucoma cases and macular hole stages. This metric directly measures the models’ ability to determine the presence of glaucoma and the severity of macular holes based on visual characteristics.

### 4.3 Anatomical Recognition

**Overall Results.** The results for anatomical recognition in Table 3 reveal that the performance of SoTA LVLMs is far from optimal. The average F1 score across all models is a mere 0.2189, highlighting a significant discrepancy between the models’

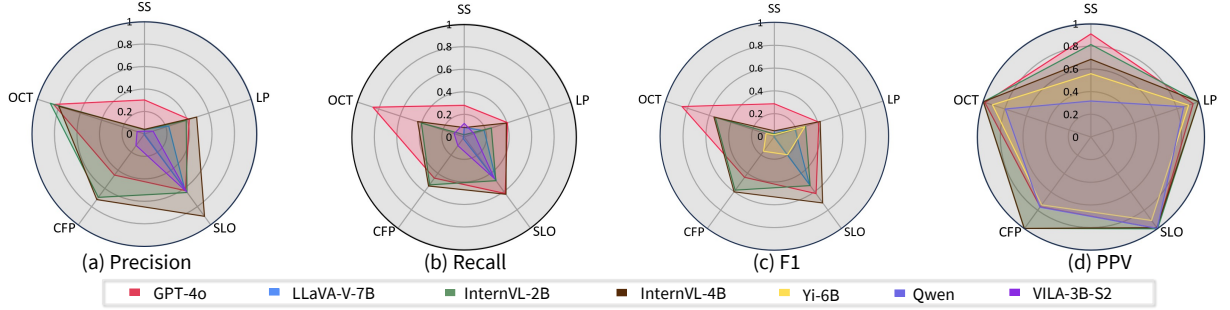


**Figure 3: Performance comparison of top-performing LVLMs across different ophthalmic imaging modalities.** The radar charts display the performance of the top-performing models, namely GPT-4o, LLaVA-V-7B, InternVL-2B, InternVL-4B, Yi-6B, Qwen, and VILA-3B-S2, for each evaluation metric (Precision, Recall, F1, and PPV) across five different ophthalmic imaging modalities: surgical scenes (SS), optical coherence tomography (OCT), color fundus photographs (CFP), scanning laser ophthalmoscopy (SLO), and eye photographs (EP).

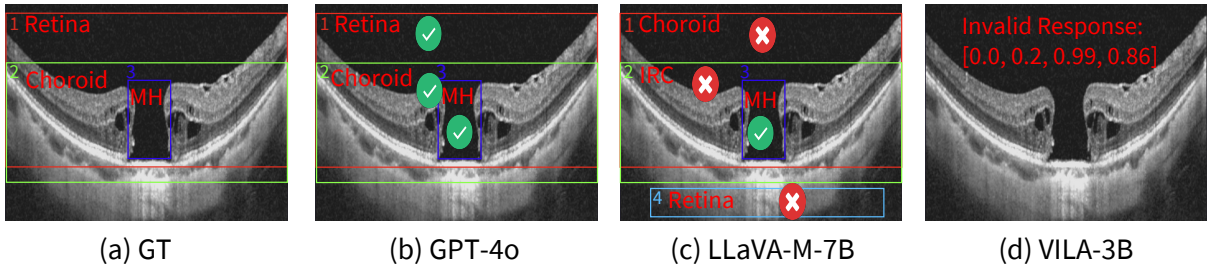


**Figure 4: Visual examples of LVLm predictions for anatomical recognition in OCT images.** The figure presents a comparison of ground truth (GT) annotations and predictions from three representative LVLMs: GPT-4o, LLaVA-M-7B, and VILA-3B. Green ticks indicate correct predictions, while red crosses mark incorrect ones. VILA-3B generates an invalid response consisting of a sequence of numbers unrelated to the task.

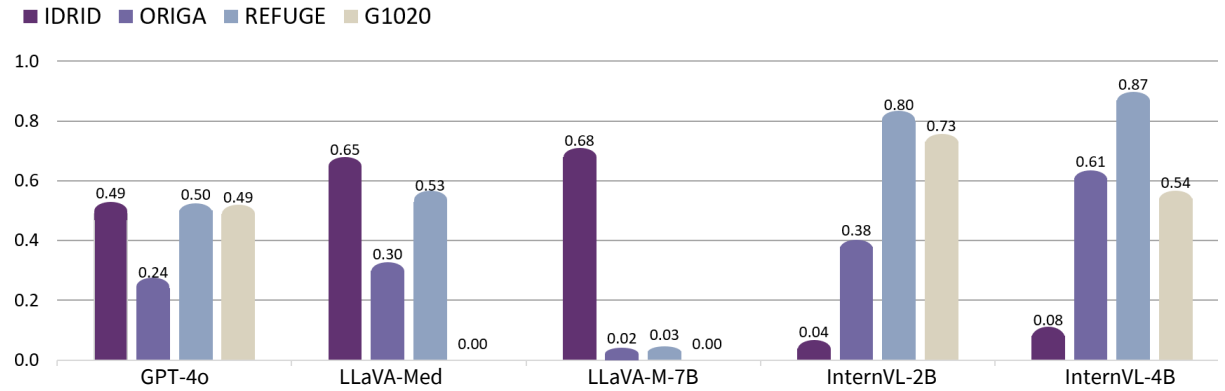


**Figure 5: Robustness analysis of LVLMs across different color fundus photograph datasets.** The bar chart displays the F1 scores of the five models (GPT-4o, LLaVA-Med, LLaVA-M-7B, InternVL-2B, and InternVL-4B) on four different color fundus photograph datasets: IDRID, ORIGA, REFUGE, and G1020.

predictions and the ground truth annotations. The best-performing model, GPT-4o, achieves an F1 score of 0.5748, which, while notably higher than the average, still indicates substantial room for improvement.

**Nuanced View.** Figure 3 provides a more nuanced view of the F1-top five models' performance

across different image types. It is crucial to note that the performance of all models, including GPT-4o, is markedly lower for complex images with a higher number of bounding boxes, such as those in the SS category. This trend suggests that the models struggle to accurately recognize and localize anatomical structures in more intricate and

information-dense images. Figure 4 presents visual examples of various responses, including correct and wrong answers, hallucination, as well as an invalid response.

**Robustness Analysis.** The performance distribution of the five best-F1 LVLMs across different CFP datasets, as depicted in Figure 5, reveals variability and inconsistency in model performance. Even for the same image modality, the models exhibit notable differences in performance depending on the specific dataset. For instance, InternVL-4B achieves a high F1 score of 0.87 on REFUGE but experiences a substantial drop in performance on IDRID, with an F1 score of only 0.04. These observations suggest that the models’ robustness and generalization ability may be limited when confronted with variations in image quality, acquisition protocols, and patient populations.

#### 4.4 Diagnosis Analysis

**Overall Results.** The evaluation results for diagnosis analysis in Table 3 demonstrate that the performance of SoTA LVLMs is far from perfect. For glaucoma detection, all models achieve an accuracy close to random guessing, indicating that they struggle to distinguish between glaucoma and non-glaucoma cases based solely on the provided ophthalmology images. In the case of macular hole staging, the average accuracy across all models is only 13.44%, suggesting a significant gap between the models’ predictions and the ground truth labels. GPT-4o, the best-performing model, achieves an accuracy of 58.97% for macular hole staging, which, while considerably higher than the average, still falls short of the desired performance for clinics.

**Error Analysis.** To better understand the limitations and failure modes of LVLMs in ophthalmology, we performed a detailed error analysis. Six primary categories emerged as follows. These categories illustrate the models’ need for better robustness, domain-specific integration, and uncertainty handling. See supplements for more detailed results.

- **Misclassification.** Models misidentify conditions or stages, leading to incorrect predictions. For example, Med-LLaVA incorrectly classified non-glaucoma images as glaucoma.
- **Failure to Abstain.** Some models fail to abstain from making predictions when presented with irrelevant or insufficient data. As shown in Figure 1, Med-LLaVA diagnosed glaucoma from an

image of a cat, which is clearly not relevant to the medical task. This error type occurs because the model should have recognized that the image is not suitable for diagnosis and refrained from making a prediction.

- **Inconsistent Reasoning.** Models provide contradictory explanations within their own predictions. For example, InternVL initially described the fundus as normal but later mentioned signs of glaucoma. This is inconsistent reasoning because the explanation contradicts itself by suggesting both a healthy and diseased state.
- **Hallucination.** Models generate details that do not exist in the input. For example, LLaVA-13B hallucinated the presence of a beard in an OCT image to justify a sex determination. This corresponds to hallucination because the beard was not present in the image, and the model invented this feature.
- **Assertion.** Models present assertive predictions without detailed explanations. For example, Yi-6B just output the glaucoma condition without further explanation despite being explicitly instructed to do so.
- **Lack of Domain-Specific Knowledge.** Models display ignorance of medical knowledge or provide medically inaccurate explanations. For example, VILA-8B assumed retinal development differs between genders, a medically unfounded statement. This error demonstrates a lack of domain-specific knowledge because the model made incorrect medical assumptions. Additionally, VILA-8B predicted a macular hole stage 5, which does not exist in the established staging system.

### 5 Conclusion

We introduced LMOD, a comprehensive benchmark for evaluating large vision-language models on ophthalmology images. LMOD encompasses a diverse range of image types and provides rich annotations for anatomical structures and diagnostic labels. Our extensive experiments with 13 state-of-the-art LVLMs revealed their limitations in fully understanding the complexities of ophthalmology images, particularly in terms of spatial reasoning, diagnostic analysis, and handling out-of-domain queries. The models struggled with anatomical recognition in complex images and exhibited inconsistent performance across different datasets. For

diagnostic analysis, the models performed close to random guessing in glaucoma detection and achieved limited accuracy in macular hole staging. Our error analysis uncovered six primary failure modes, highlighting the need for improved robustness, domain-specific integration, and uncertainty handling. These findings underscore the necessity for targeted adaptations and the incorporation of expert knowledge to bridge the gap between general-purpose vision-language models and the specialized requirements of ophthalmology.

## References

Josh Achiam, Steven Adler, Sandhini Agarwal, Lama Ahmad, Ilge Akkaya, Florencia Leoni Aleman, Diogo Almeida, Janko Altenschmidt, Sam Altman, Shyamal Anadkat, et al. 2023. Gpt-4 technical report. *OpenAI*.

Fares Antaki, Samir Touma, Daniel Milad, Jonathan El-Khoury, and Renaud Duval. 2023. Evaluating the performance of chatgpt in ophthalmology: an analysis of its successes and shortcomings. *Ophthalmology science*, 3(4):100324.

Stanislaw Antol, Aishwarya Agrawal, Jiasen Lu, Margaret Mitchell, Dhruv Batra, C Lawrence Zitnick, and Devi Parikh. 2015. Vqa: Visual question answering. In *Proceedings of the IEEE international conference on computer vision*, pages 2425–2433.

Jinze Bai, Shuai Bai, Shusheng Yang, Shijie Wang, Sinan Tan, Peng Wang, Junyang Lin, Chang Zhou, and Jingren Zhou. 2023. Qwen-vl: A frontier large vision-language model with versatile abilities. *arXiv preprint arXiv:2308.12966*.

Muhammad Naseer Bajwa, Gur Amrit Pal Singh, Wolfgang Neumeier, Muhammad Imran Malik, Andreas Dengel, and Sheraz Ahmed. 2020. G1020: A benchmark retinal fundus image dataset for computer-aided glaucoma detection. In *2020 International Joint Conference on Neural Networks (IJCNN)*, pages 1–7. IEEE.

Bjorn Kaijun Betzler, Haichao Chen, Ching-Yu Cheng, Cecilia S Lee, Guochen Ning, Su Jeong Song, Aaron Y Lee, Ryo Kawasaki, Peter van Wijngaarden, Andrzej Grzybowski, et al. 2023. Large language models and their impact in ophthalmology. *The Lancet Digital Health*, 5(12):e917–e924.

Tom Brown, Benjamin Mann, Nick Ryder, Melanie Subbiah, Jared D Kaplan, Prafulla Dhariwal, Arvind Neelakantan, Pranav Shyam, Girish Sastry, Amanda Askell, et al. 2020. Language models are few-shot learners. *Advances in neural information processing systems*, 33:1877–1901.

D Cavan, L Makaroff, J da Rocha Fernandes, M Sylwanowicz, P Ackland, J Conlon, D Chaney, A Malhi, and J Barratt. 2017. The diabetic retinopathy barometer study: global perspectives on access to and experiences of diabetic retinopathy screening and treatment. *Diabetes research and clinical practice*, 129:16–24.

Qingyu Chen, Jingcheng Du, Yan Hu, Vipina Kuttichi Keloth, Xueqing Peng, Kalpana Raja, Rui Zhang, Zhiyong Lu, and Hua Xu. 2023. Large language models in biomedical natural language processing: benchmarks, baselines, and recommendations. *arXiv preprint arXiv:2305.16326*.

Zhe Chen, Jiannan Wu, Wenhui Wang, Weijie Su, Guo Chen, Sen Xing, Muyan Zhong, Qinglong Zhang, Xizhou Zhu, Lewei Lu, Bin Li, Ping Luo, Tong Lu, Yu Qiao, and Jifeng Dai. 2024. Internvl: Scaling up vision foundation models and aligning for generic visual-linguistic tasks. *IEEE/CVF Conference on Computer Vision and Pattern Recognition (CVPR)*.

Jan Clusmann, Fiona R Kolbinger, Hannah Sophie Muti, Zunamys I Carrero, Jan-Niklas Eckardt, Narmen Ghaffari Laleh, Chiara Maria Lavinia Löffler, Sophie-Caroline Schwarzkopf, Michaela Unger, Gregory P Veldhuizen, et al. 2023. The future landscape of large language models in medicine. *Communications medicine*, 3(1):141.

G Currie, C Singh, T Nelson, C Nabasenja, Y Al-Hayek, and K Spuur. 2023. Chatgpt in medical imaging higher education. *Radiography*, 29(4):792–799.

Luigi De Angelis, Francesco Baglivo, Guglielmo Arzilli, Gaetano Pierpaolo Privitera, Paolo Ferragina, Alberto Eugenio Tozzi, and Caterina Rizzo. 2023. Chatgpt and the rise of large language models: the new ai-driven infodemic threat in public health. *Frontiers in public health*, 11:1166120.

Jeffrey De Fauw, Joseph R Ledsam, Bernardino Romera-Paredes, Stanislav Nikolov, Nenad Tomasev, Sam Blackwell, Harry Askham, Xavier Glorot, Brendan O’Donoghue, Daniel Visentin, et al. 2018. Clinically applicable deep learning for diagnosis and referral in retinal disease. *Nature Medicine*, 24(9):1342–1350.

JL Demer. 2006. Anatomical diagnosis.

Mohamed Elkholy and Marwa A Marzouk. 2024. Deep learning-based classification of eye diseases using convolutional neural network for oct images. *Frontiers in Computer Science*, 5:1252295.

Negin Ghamsarian, Yosuf El-Shabrawi, Sahar Nasir-ihaghghi, Doris Putzgruber-Adamitsch, Martin Zinkernagel, Sebastian Wolf, Klaus Schoeffmann, and Raphael Sznitman. 2024. Cataract-1k dataset for deep-learning-assisted analysis of cataract surgery videos. *Scientific Data*, 11(1):373.

Yash Goyal, Tejas Khot, Douglas Summers-Stay, Dhruv Batra, and Devi Parikh. 2017. Making the v in vqa matter: Elevating the role of image understanding in visual question answering. In *Proceedings of the IEEE conference on computer vision and pattern recognition*, pages 6904–6913.

Yangyang Guo, Fangkai Jiao, Zhiqi Shen, Liqiang Nie, and Mohan Kankanhalli. 2024. Unk-vqa: A dataset and a probe into the abstention ability of multi-modal large models. *IEEE Transactions on Pattern Analysis and Machine Intelligence*.

Ming Hu, Peng Xia, Lin Wang, Siyuan Yan, Feilong Tang, Zhongxing Xu, Yimin Luo, Kaimin Song, Jurgen Leitner, Xuelian Cheng, et al. 2024. Ophnet: A large-scale video benchmark for ophthalmic surgical workflow understanding. *arXiv preprint arXiv:2406.07471*.

Songtao Jiang, Tuo Zheng, Yan Zhang, Yeying Jin, and Zuozhu Liu. 2024. Moe-tinymed: Mixture of experts for tiny medical large vision-language models. *arXiv preprint arXiv:2404.10237*.

Vishal Kaushal, Nishant Singh Hada, and Sangeeta Sharma. 2023. Eye disease detection through image classification using federated learning. *SN Computer Science*, 4(6):836.

Tiarnan DL Keenan, Qingyu Chen, Elvira Agrón, Yih-Chung Tham, Jocelyn Hui Lin Goh, Xiaofeng Lei, Yi Pin Ng, Yong Liu, Xinxing Xu, Ching-Yu Cheng, et al. 2022. Deeplensnet: deep learning automated diagnosis and quantitative classification of cataract type and severity. *Ophthalmology*, 129(5):571–584.

Saad M Khan, Xiaoxuan Liu, Siddharth Nath, Edward Korot, Livia Faes, Siegfried K Wagner, Pearse A Keane, Neil J Sebire, Matthew J Burton, and Alastair K Denniston. 2021. A global review of publicly available datasets for ophthalmological imaging: barriers to access, usability, and generalisability. *The Lancet Digital Health*, 3(1):e51–e66.

Tiffany H Kung, Morgan Cheatham, Arielle Medenilla, Czarina Sillos, Lorie De Leon, Camille Elepaño, Maria Madriaga, Rimel Aggabao, Giezel Diaz-Candido, James Maningo, et al. 2023. Performance of chatgpt on usmle: potential for ai-assisted medical education using large language models. *PLoS digital health*, 2(2):e0000198.

Bohao Li, Yuying Ge, Yixiao Ge, Guangzhi Wang, Rui Wang, Ruimao Zhang, and Ying Shan. 2024a. Seed-bench: Benchmarking multimodal large language models. In *Proceedings of the IEEE/CVF Conference on Computer Vision and Pattern Recognition*, pages 13299–13308.

Chunyuan Li, Cliff Wong, Sheng Zhang, Naoto Usuyama, Haotian Liu, Jianwei Yang, Tristan Naumann, Hoifung Poon, and Jianfeng Gao. 2024b. Llava-med: Training a large language-and-vision assistant for biomedicine in one day. 36.

Zhi Wei Lim, Krithi Pushpanathan, Samantha Min Er Yew, Yien Lai, Chen-Hsin Sun, Janice Sing Harn Lam, David Ziyou Chen, Jocelyn Hui Lin Goh, Marcus Chun Jin Tan, Bin Sheng, et al. 2023. Benchmarking large language models’ performances for myopia care: a comparative analysis of chatgpt-3.5, chatgpt-4.0, and google bard. *EBioMedicine*, 95.

Ji Lin, Hongxu Yin, Wei Ping, Yao Lu, Pavlo Molchanov, Andrew Tao, Huizi Mao, Jan Kautz, Mohammad Shoeybi, and Song Han. 2023. Vila: On pre-training for visual language models. *arXiv preprint arXiv:2312.07533*.

Tsung-Yi Lin, Michael Maire, Serge Belongie, James Hays, Pietro Perona, Deva Ramanan, Piotr Dollár, and C Lawrence Zitnick. 2014. Microsoft coco: Common objects in context. In *Computer Vision–ECCV 2014: 13th European Conference, Zurich, Switzerland, September 6–12, 2014, Proceedings, Part V 13*, pages 740–755. Springer.

Haotian Liu, Chunyuan Li, Qingyang Wu, and Yong Jae Lee. 2024. Visual instruction tuning. *Advances in Neural Information Processing Systems (NeurIPS)*, 36.

Yiheng Liu, Tianle Han, Siyuan Ma, Jiayue Zhang, Yuanyuan Yang, Jiaming Tian, Hao He, Antong Li, Mengshen He, Zhengliang Liu, et al. 2023. Summary of chatgpt-related research and perspective towards the future of large language models. *Meta-Radiology*, page 100017.

Pan Lu, Hritik Bansal, Tony Xia, Jiacheng Liu, Chunyuan Li, Hannaneh Hajishirzi, Hao Cheng, Kai-Wei Chang, Michel Galley, and Jianfeng Gao. 2023. Mathvista: Evaluating mathematical reasoning of foundation models in visual contexts. *International Conference on Learning Representation (ICLR)*.

Yan Luo, Yu Tian, Min Shi, Louis R Pasquale, Lucy Q Shen, Nazlee Zebardast, Tobias Elze, and Mengyu Wang. 2024. Harvard glaucoma fairness: a retinal nerve disease dataset for fairness learning and fair identity normalization. *IEEE Transactions on Medical Imaging*.

David C Neely, Kevin J Bray, Carrie E Huisingsh, Mark E Clark, Gerald McGwin, and Cynthia Owsley. 2017. Prevalence of undiagnosed age-related macular degeneration in primary eye care. *JAMA ophthalmology*, 135(6):570–575.

World Health Organization. 2023. *Blindness and vision impairment*. Accessed: [Insert access date here].

José Ignacio Orlando, Huazhu Fu, João Barbosa Breda, Karel Van Keer, Deepti R Bathula, Andrés Diaz-Pinto, Ruogu Fang, Pheng-Ann Heng, Jeyoung Kim, JoonHo Lee, et al. 2020. Refuge challenge: A unified framework for evaluating automated methods for glaucoma assessment from fundus photographs. *Medical image analysis*, 59:101570.

Yifan Peng, Shazia Dharssi, Qingyu Chen, Tiarnan D Keenan, Elvira Agrón, Wai T Wong, Emily Y Chew, and Zhiyong Lu. 2019. Deepseenet: a deep learning model for automated classification of patient-based age-related macular degeneration severity from color fundus photographs. *Ophthalmology*, 126(4):565–575.

Ryan Poplin, Avinash V Varadarajan, Katy Blumer, Yun Liu, Michael V McConnell, Greg S Corrado, Lily Peng, and Dale R Webster. 2018. Prediction of cardiovascular risk factors from retinal fundus photographs via deep learning. *Nature biomedical engineering*, 2(3):158–164.

Porwal Prasanna, Pachade Samiksha, Kamble Ravi, Kokare Manesh, D Girish, S Vivek, and Meriaudeau Fabrice. 2018. Indian diabetic retinopathy image dataset (idrid). *IEEE Dataport*, 2.

PupiUp. 2023. [cau001 dataset](#). *Roboflow Universe*. Visited on 2024-06-03.

Ziyuan Qin, Huahui Yi, Qicheng Lao, and Kang Li. 2022. Medical image understanding with pretrained vision language models: A comprehensive study. *arXiv preprint arXiv:2209.15517*.

Alec Radford, Karthik Narasimhan, Tim Salimans, Ilya Sutskever, et al. 2018. Improving language understanding by generative pre-training.

Alec Radford, Jeffrey Wu, Rewon Child, David Luan, Dario Amodei, Ilya Sutskever, et al. 2019. Language models are unsupervised multitask learners. *OpenAI blog*, 1(8):9.

SRM University Ramapuram. 2023. Cataract detection 2 dataset. *Roboflow Universe*. Visited on 2024-06-03.

Yih-Chung Tham, Xiang Li, Tien Y Wong, Harry A Quigley, Tin Aung, and Ching-Yu Cheng. 2014. Global prevalence of glaucoma and projections of glaucoma burden through 2040: a systematic review and meta-analysis. *Ophthalmology*, 121(11):2081–2090.

Shubo Tian, Qiao Jin, Lana Yeganova, Po-Ting Lai, Qingqing Zhu, Xiuying Chen, Yifan Yang, Qingyu Chen, Won Kim, Donald C Comeau, et al. 2024. Opportunities and challenges for chatgpt and large language models in biomedicine and health. *Briefings in Bioinformatics*, 25(1):bbad493.

Daniel Shu Wei Ting, Louis R Pasquale, Lily Peng, John Peter Campbell, Aaron Y Lee, Rajiv Raman, Gavin Siew Wei Tan, Leopold Schmetterer, Pearse A Keane, and Tien Yin Wong. 2019. Artificial intelligence and deep learning in ophthalmology. *British Journal of Ophthalmology*, 103(2):167–175.

Rohit Varma, Paul P Lee, Ivan Goldberg, and Sameer Kotak. 2011. An assessment of the health and economic burdens of glaucoma. *American journal of ophthalmology*, 152(4):515–522.

Shanshan Wang, Cheng Li, Rongpin Wang, Zaiyi Liu, Meiyun Wang, Hongna Tan, Yaping Wu, Xinfeng Liu, Hui Sun, Rui Yang, et al. 2021. Annotation-efficient deep learning for automatic medical image segmentation. *Nature Communications*, 12(1):5915.

Sean Wu, Michael Koo, Lesley Blum, Andy Black, Liyo Kao, Zhe Fei, Fabien Scalzo, and Ira Kurtz. 2024. Benchmarking open-source large language models, gpt-4 and claude 2 on multiple-choice questions in nephrology. *NEJM AI*, 1(2):A1dbp2300092.

Hanguang Xiao, Feizhong Zhou, Xingyue Liu, Tianqi Liu, Zhipeng Li, Xin Liu, and Xiaoxuan Huang. 2024. A comprehensive survey of large language models and multimodal large language models in medicine. *arXiv preprint arXiv:2405.08603*.

Yunfei Xie, Ce Zhou, Lang Gao, Juncheng Wu, Xianhang Li, Hong-Yu Zhou, Sheng Liu, Lei Xing, James Zou, Cihang Xie, et al. 2024. Medtrinity-25m: A large-scale multimodal dataset with multi-granular annotations for medicine. *arXiv preprint arXiv:2408.02900*.

Xin Ye, Shucheng He, Xiaxing Zhong, Jiafeng Yu, Shangchao Yang, Yingjiao Shen, Yiqi Chen, Yaqi Wang, Xingru Huang, and Lijun Shen. 2023. Oimhs: An optical coherence tomography image dataset based on macular hole manual segmentation. *Scientific Data*, 10(1):769.

Alex Young, Bei Chen, Chao Li, Chengan Huang, Ge Zhang, Guanwei Zhang, Heng Li, Jiangcheng Zhu, Jianqun Chen, Jing Chang, et al. 2024. Yi: Open foundation models by 01. ai. *arXiv preprint arXiv:2403.04652*.

Xiang Yue, Yuansheng Ni, Kai Zhang, Tianyu Zheng, Ruqi Liu, Ge Zhang, Samuel Stevens, Dongfu Jiang, Weiming Ren, Yuxuan Sun, Cong Wei, Botao Yu, Ruibin Yuan, Renliang Sun, Ming Yin, Boyuan Zheng, Zhenzhu Yang, Yibo Liu, Wenhao Huang, Huan Sun, Yu Su, and Wenhui Chen. 2024. Mmmu: A massive multi-discipline multimodal understanding and reasoning benchmark for expert agi. In *IEEE/CVF Conference on Computer Vision Pattern Recognition (CVPR)*.

Jiawei Zhang, Tianyu Pang, Chao Du, Yi Ren, Bo Li, and Min Lin. 2024a. Benchmarking large multimodal models against common corruptions. *arXiv preprint arXiv:2401.11943*.

Yi-Fan Zhang, Huanyu Zhang, Haochen Tian, Chaoyou Fu, Shuangqing Zhang, Junfei Wu, Feng Li, Kun Wang, Qingsong Wen, Zhang Zhang, et al. 2024b. Mme-realworld: Could your multimodal llm challenge high-resolution real-world scenarios that are difficult for humans? *arXiv preprint arXiv:2408.13257*.

Zhuo Zhang, Feng Shou Yin, Jiang Liu, Wing Kee Wong, Ngan Meng Tan, Beng Hai Lee, Jun Cheng, and Tien Yin Wong. 2010. Origalight: An online retinal fundus image database for glaucoma analysis and research. In *2010 Annual International Conference of the IEEE Engineering in Medicine and Biology*, pages 3065–3068. IEEE.

Yukun Zhou, Mark A Chia, Siegfried K Wagner, Murat S Ayhan, Dominic J Williamson, Robbert R

Struyven, Timing Liu, Moucheng Xu, Mateo G Lozano, Peter Woodward-Court, et al. 2023. A foundation model for generalizable disease detection from retinal images. *Nature*, 622(7981):156–163.